Key Engineering Materials
ISSN: 1662-9795, Vol. 926, pp 65-79
doi:10.4028/p-ob7dg7

Submitted: 2021-11-30
Revised: 2022-01-27
Accepted: 2022-02-18
Online: 2022-07-22

Laser Metal Deposition with Coaxial Wire Feeding for the Automated and Reliable Build-Up of Solid Metal Parts

Christian Bernauer[1,a*], Thomas Merk[1,b], Avelino Zapata[1,c] and Michael F. Zaeh[1,d]

[1]Technical University of Munich, TUM School of Engineering and Design, Institute for Machine Tools and Industrial Management (iwb), Boltzmannstrasse 15, 85748 Garching, Germany

[a]christian.bernauer@iwb.tum.de, [b]thomas.merk@tum.de, [c]avelino.zapata@iwb.tum.de, [d]michael.zaeh@iwb.tum.de

Keywords: laser metal deposition, multi-layer deposition, annular laser beam, directed energy deposition, coaxial wire feeding

Abstract. Due to their outstanding characteristics, additive manufacturing processes are attracting increasing industrial interest. Among these processes, laser metal deposition (LMD) is an innovative technology for the production of metal components. In order to create three-dimensional parts, wire or powder is deposited layer-wise onto a substrate. When wire is used as feedstock, major drawbacks of the powder-based process, such as the low material usage, contamination of the process cell with metal powder, and health or safety issues, can be overcome or even avoided. In addition, recent developments in laser optics allow for a coaxial wire feeding in the center of an annular laser beam. This eliminates the strong directional dependence of the process when feeding the wire laterally. However, wire-based LMD is highly sensitive to process disturbances, which impedes its broader industrial application. Since it is necessary to completely melt the fed wire to achieve a stable process, self-regulating effects such as overspray in powder-based LMD are not present.

In contrast to the widely investigated thin walls, the build-up of multi-track solid structures poses a particular challenge. Therefore, process strategies for producing such solid structures are presented in this paper. The experiments were carried out using a laser processing head that enables coaxial wire feeding (CoaxPrinter, Precitec). By systematically varying the lateral overlap between adjacent weld beads, it was shown that an optimum exists at which minimum surface waviness is achieved. Based on this, defect-free multi-layer solid components could be generated in a reproducible manner. During the process, the melt pool temperature was evaluated using a pyrometer. Furthermore, a microscopic examination of the resulting parts was conducted. The results obtained show the need for process monitoring and control, for which a novel and holistic approach has been developed.

Introduction

Laser metal deposition (LMD) is an emerging additive manufacturing technology that enables significantly higher build rates than the widely used processes employing a powder bed. In LMD processes, powder or wire is continuously and locally fed to a substrate into a laser-induced molten pool. By repeating the application layer by layer, three-dimensional metal components can be produced. This offers great potential for applications in various industries, such as aerospace, tooling, oil and gas, and automotive [1]. Across these industries, stainless steels are among the most commonly used materials [2]. For the manufacturing of metal parts, the use of wire as feedstock offers several advantages over the use of powder. Using wire enables a material utilization of 100 % while avoiding hazardous effects of metal dust on the operator and the environment [3]. In wire-based LMD, the filler material is typically fed laterally to a Gaussian laser beam. This results in a strong directional dependency of the process, as the wire is fed from the front, the back, or the side, depending on the direction of movement [4]. However, recent developments of laser processing optics also allow for a directionally independent process by feeding the wire either in the center of several single beams [5–8] or inside an annular laser beam [9–11]. Despite the advantage of directional independence, coaxial

wire-based LMD is highly sensitive to process disturbances, which impedes its broader industrial application.

To achieve a stable process, precise tuning of the process parameters is required. Otherwise, the typical defect types as described by Motta et al. [10] occur. In the case of stubbing, wire fragments that have not been melted adhere to the substrate due to insufficient energy input. In contrast, in the case of dripping, droplets are formed at the end of the fed wire as a result of excessive energy input. Furthermore, the self-regulating effects due to overspray as described by Zhu et al. [12] and Donadello et al. [13] for powder-based LMD are not present since it is necessary to fully melt the fed wire. The expected or theoretical layer height must consequently be very close to the actual layer height to keep the distance between the laser processing head and the surface of the part constant during the build-up [14].

For thin-walled structures, which were most commonly studied in literature [15], an improper height adjustment can be self-compensated to a minor extent. If the height increment is too small, the laser beam is defocused more than the initial setpoint, which leads to a wider melt pool and thus to a reduced layer height due to the constant volume of the fed material. Likewise, if the height increment is too large, the melt pool is narrower, resulting in a greater layer height [16]. In contrast, this effect does not apply to the build-up of multi-track solid structures, which are crucial for the production of many industrially relevant components. With such solid structures, additional complexity is added since the lateral overlap of adjacent weld beads, the deposition pattern, and the increased heat accumulation in the part must also be considered. It should be noted that the directional independence of coaxial wire feeding offers a decisive advantage in the build-up of complex solid components since this requires frequent changes in the orientation of the tracks.

Starting from the first layer, the lateral overlap of adjacent tracks is a crucial parameter for a stable build-up. The objective should be to achieve minimal waviness of the layer surface to enable defect-free deposition of the subsequent layers. In this context, the term waviness must be distinguished from the term roughness, as irregularities in the order of magnitude of roughness only have a minor influence on the process.

Various works investigated the deposition of multi-track layers as well as the subsequent build-up of solid structures. The degree of overlap commonly refers to the proportional width of one bead overlapped when the adjacent bead is deposited. For the coating of mild steel using Inconel 625 and Thermanite 2509, it was shown by Pajukoski et al. [17] that an insufficient degree of overlap (<50 %) produced excessive dilution, while a large degree of overlap (>60 %) resulted in high porosity. Budde et al. [18] employed hot-wire LMD for the cladding of AISI 316L with high carbon steel AISI 52100. The process parameters as well as the degree of overlap between the weld beads were varied, and the claddings were investigated using cross-sections. Pore-free parameter sets were determined, although these were associated with a high degree of dilution. Kelbassa et al. [19] established a process window for the deposition of Inconel 718 and Ti6Al4V wire employing a coaxial laser processing head. Different degrees of overlap were tested and the surface waviness was assessed via cross-sections. Subsequently, cuboids with eight layers were built up, where material accumulation at the edges occurred due to the chosen path strategy. A similar procedure was utilized by Madarieta-Churruca et al. [8] for the deposition of AISI 316L stainless steel. By using a proper layer height and adapted path strategies, multi-layer solid structures could be built up. Oliari et al. [20] investigated the degree of overlap for LMD with lateral wire feeding by depositing layers with three tracks each. In this study, alloy steel (42CrMo4) was used as substrate material and AISI H11 tool steel as feedstock. With the selected degree of overlap, parts with up to ten layers could be built. However, a detailed investigation of the degree of overlap proved to be difficult due to the small number of tracks.

Furthermore, different models on the degree of overlap for multi-track wire and arc additive manufacturing (WAAM) have been established [21–25]. According to theory, a planar surface is obtained when the overlap area of two weld beads in a cross-section is equal to the area of the valley between the beads. However, it was shown that an ideally flat surface cannot be achieved [25]. In addition, the theoretically optimized distance between beads does not necessarily produce the lowest

possible waviness since other influences such as the energy input or the deposited material also affect the result.

In the existing studies on the degree of overlap, only single cross-sections were used for estimating the resulting surface waviness. However, no detailed quantification of the waviness for wire-based LMD has been performed so far. In the work presented in this paper, an approach on how to select the degree of overlap for achieving a minimum surface waviness was investigated. Based on this, multi-track multi-layer parts are produced. Even if the process parameters are precisely tuned, instabilities may arise due to the sensitivity of wire-based LMD to disturbances. To compensate for these, a novel approach for an online monitoring system as well as for a multivariable closed-loop process control based on it is presented.

Materials and Methods

Materials. For the experiments, plates of austenitic stainless steel AISI 304 (100 mm×100 mm ×10 mm) were used as substrate material. The plates were cleaned with isopropanol to remove existing contaminants. Stainless steel ER316LSi wire with a diameter of 1 mm served as feedstock material. The chemical compositions are given in Table 1.

Table 1: Chemical composition of the wire and the substrate material (wt%)

Element	Cr	Ni	Mo	Mn	Si	C	P	S	Fe
Wire	18.38	11.37	2.52	1.82	0.67	0.013	0.018	0.018	Bal.
Substrate	17.0–19.0	8.0–11.0	–	≤2.0	≤1.0	≤0.07	≤0.035	≤0.03	Bal.

Experimental Setup. The experimental setup is depicted in Figure 1. Laser radiation with a wavelength of 1030 nm was generated by a 4 kW disk laser (TruDisk 4001, TRUMPF GmbH & Co. KG, Ditzingen, Germany) operating in continuous wave (cw) mode. Through a 600 µm optical fiber, the radiation was transmitted to the laser processing head (CoaxPrinter, Precitec GmbH & Co. KG, Gaggenau, Germany). Here, the beam shaping took place, which allowed for coaxial feeding of the wire within an annular beam profile. Thus, a direction-independent LMD process was enabled. To provide the feedstock, an industrial wire feeding unit (DIX FDE-PN 100 L, DINSE GmbH, Hamburg, Germany) was used. The curvature of the wire, which was delivered in a coil, was compensated by a precisely adjusted two-plane wire straightening unit. The laser processing head was moved by a six-axis industrial robot (KR 60, KUKA AG, Augsburg, Germany) with a maximum payload of 60 kg, which was actuated by a robotic control system (KR C4, KUKA AG, Augsburg, Germany). A pyrometer (METIS M322, Sensortherm GmbH, Steinbach, Germany) in one-color mode (sensitive in the range of 1.45 – 1.65 µm) with a temperature measurement range of 600 – 2300 °C was mounted to the laser processing head for a coaxial measurement of the melt pool temperature during the process. The calibration of the pyrometer to the surface temperature of the melt pool has been discussed in detail in previous work [26].

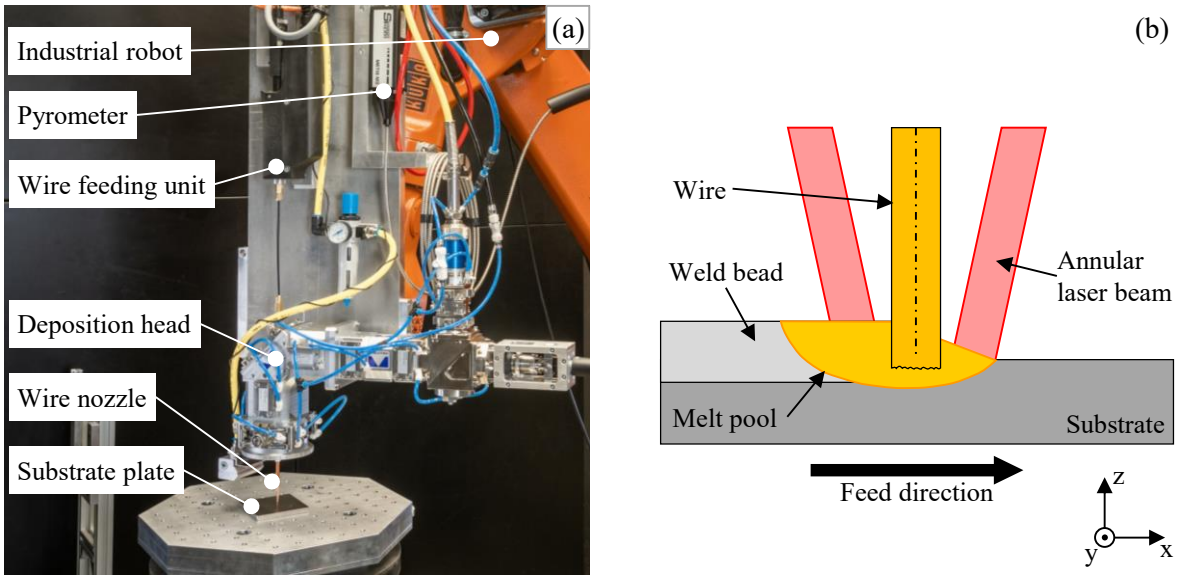

Figure 1: Laser metal deposition process with coaxial wire feeding: (a) experimental setup; (b) schematic illustration of the process zone

Experimental Procedure. To investigate the surface waviness of a single layer, 15 laterally overlapping weld beads were deposited in a zigzag pattern, as shown in Figure 2a. An interruption of the process between individual tracks was omitted to avoid influences of the initial transient phase on the bead geometry. The laser power was varied on the three levels 1200 W, 1600 W, and 2000 W. In each case, the remaining process parameters traverse speed and wire feed rate were adjusted based on preliminary studies so that a stable deposition was obtained for single-track beads. Thus, with a higher laser power, the other parameter values were also increased to avoid excessive heat input and the associated defect pattern of dripping [10]. The applied parameter sets denoted as A, B, and C are given in Table 2. During all experiments, a constant shielding gas flow (Argon) of 20 l/min was used. The focal position was set at −6 mm so that the focal point was below the surface of the substrate. This resulted in an outer and inner diameter of the ring-shaped laser spot of 2.75 mm and 1.50 mm, respectively. The measurement spot of the pyrometer was adjusted using the fiber optics so that an outer diameter of 2.4 mm and an inner diameter of 1.3 mm was obtained at this focal position, minimizing disturbances of the signal due to the fed wire [26].

Table 2: Process parameters for the deposition of a single layer with multiple tracks

Varied parameters	Unit	Parameter set		
		A	B	C
Laser power P_L	W	1200	1600	2000
Traverse speed v_t	m/min	1.0	1.3	1.5
Wire feed rate v_w	m/min	1.1	1.2	1.3
Fixed parameters				
Focal position f	mm		−6	
Shielding gas flow	l/min		20	

The width of a single bead together with the distance between the tracks determines the degree of overlap. As shown schematically in Figure 2b, the degree of overlap is defined as the lateral proportion of a bead that is overlapped during the deposition of the next bead [20]. However, since the overlap area in a cross-section also depends on the bead shape, the degree of overlap is not necessarily suitable for a comparison with literature values. Therefore, in the following, the distance

d_t between the center lines of adjacent beads, also denoted as track distance, will be used. For each parameter set, the track distance was reduced in steps of 0.1 mm, starting at a distance of 1.7 mm. At this maximum distance, significant valleys were still apparent between the beads. As soon as a significant increase in defects occurred due to the large overlap, the test sequence was terminated for the respective parameter set.

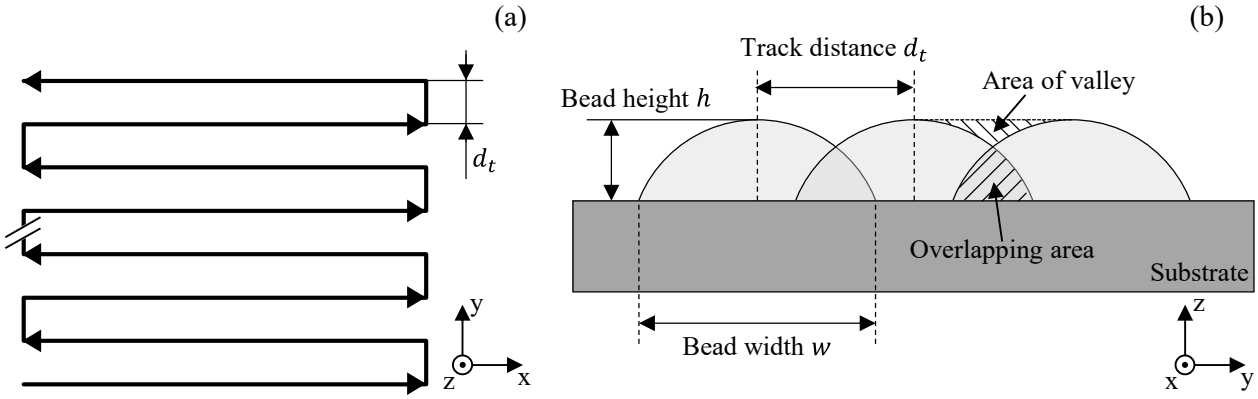

Figure 2: (a) deposition pattern for a single layer; (b) Schematic visualization of laterally overlapping beads and their geometric parameters [23]

Characterizations. The topography of the applied layers was measured using a 3D profilometer (VR-3100, Keyence Corporation, Osaka, Japan). Thermal distortions of the substrate plates caused by the process were compensated for in the included software. For the investigation of the surface waviness, a reference area with a width of 10 mm along the direction of the tracks was uniformly selected for each sample, as illustrated in Figure 3. Within this area, the standard deviation was computed over the z-coordinates of all included points, serving as a measure for the waviness. In each case, the outermost weld beads were not considered. Due to the high number of points within the considered areas, an objective and representative quantification of the waviness is enabled, which clearly distinguishes this procedure from previous works. An example for the analyzed region of the height profile is shown in Figure 3.

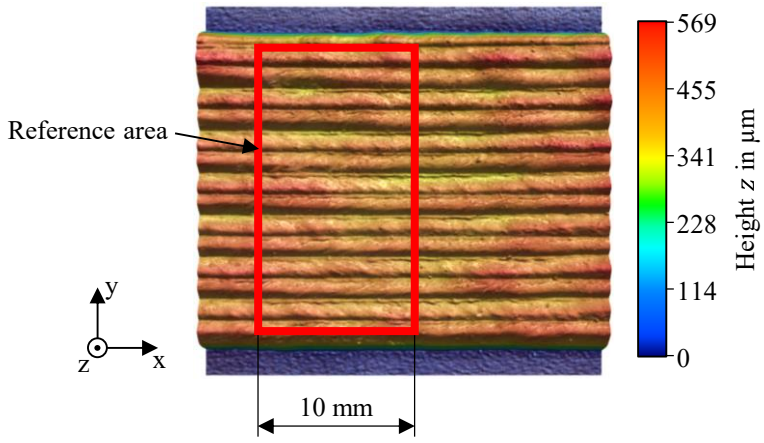

Figure 3: Exemplary surface profile of a single layer containing the reference area with a width of 10 mm

A laser scanning confocal microscope (VK-X 1000, Keyence Corporation, Osaka, Japan) was used to examine of the cross-sections and to determine the geometric features of the individual weld beads. Furthermore, a scanning electron microscope (JSM-IT200, JEOL Ltd., Akishima, Japan) with an integrated unit for energy dispersive X-ray spectroscopy (EDS) was employed to analyze the elemental composition of the built-up material.

Results and Discussion

Distance between Weld Beads. Since the geometry of a single weld bead significantly influences the resulting surface characteristics at a given track distance, this should initially be considered separately. Figure 4 shows cross-sections of single beads for the three investigated parameter sets. Based on the respective geometry, the theoretically optimum track distance $\hat{d}_t$ can be computed. Therefore, the track distance is set in such a way that the overlapping area and the area of the valley are equal (see Figure 2b) [23]. According to Shi et al. [16], for LMD with coaxial wire feeding, the geometry of a bead can be described by a circular arc in good approximation. This also holds true to the three parameter sets used in this study, as illustrated in Figure 4. Knowing the width w, the height h and the radius R, the theoretically optimum track distance of two adjacent circular arc beads can be calculated as follows [23]:

$$\hat{d}_t = \frac{1}{2h}\left(2R^2 arcsin\frac{w}{2R} + wh - wR\right) \tag{1}$$

This leads to optimum track distances of 1.73 mm, 1.78 mm, and 1.78 mm for parameter sets A, B, and C, respectively.

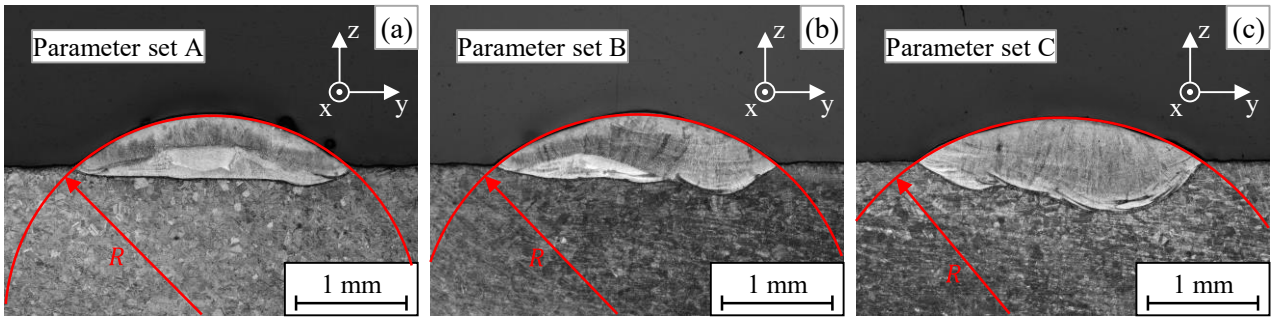

Figure 4: Contour of a single bead approximated by a circular arc together with the geometric specifications for parameter sets A (a), B (b), and C (c)

In practice, to achieve minimum waviness for a deposited layer, the set track distance must result in a minimum standard deviation σ of the z-coordinates for the measuring points within the reference area. Figure 5 shows the respective mean values and standard deviations obtained from the three test series conducted.

For the mean values (cf. Figure 5a), which serve as a measure of the resulting layer height, a distinct trend is apparent, with the height of the deposited layer increasing as the spacing between the beads decreases. The exponential curve can be explained by the fact that with higher degrees of overlap, a further reduction in the distance between tracks also leads to a higher change in the overlapping area in the cross-section due to the convex geometry of the beads (see Figure 2b). Since the entire volume of the fed wire is deposited, this corresponds to a greater increase in the height.

For parameter sets A and B, the standard deviations of the z-coordinates exhibit a minimum at a distance of 1.1 mm and 1.0 mm, respectively, while it increases for higher as well as for lower track distances. In relation to the respective bead widths, these values correspond to a degree of overlap of 44 % and 39 %. The actual optimum track distance is thus considerably less than the theoretically calculated one. This is because various physical phenomena such as gravity, viscosity, and surface tension also influence the bead formation [25]. Due to the many uncertainties that have to be considered when modeling the optimum track distance, in practice, using the presented approach may be significantly more efficient. This clearly shows that, depending on the chosen parameter set, there is an optimum for the track distance at which the smoothest surface can be achieved. In the

investigated parameter range resulting in a stable deposition, the standard deviation for large and small track distances was approximately twice as high as for the optimum track distance in each case.

When investigating parameter set C, the test series was stopped prematurely at a track distance of 1.3 mm due to frequent defects, resulting in only five samples. In this case, although the parameter set yielded a stable process and defect-free beads for single tracks, overheating occurred when depositing adjacent beads due to the high energy input. As a result, the contact between the wire and the workpiece was repeatedly interrupted, leading to frequent droplet formations.

Since parameter set B exhibited the lowest waviness, it was selected for the further investigations. In addition, when using parameter set B a higher deposition rate was achieved than using parameter set A, which is preferable in terms of an economical process.

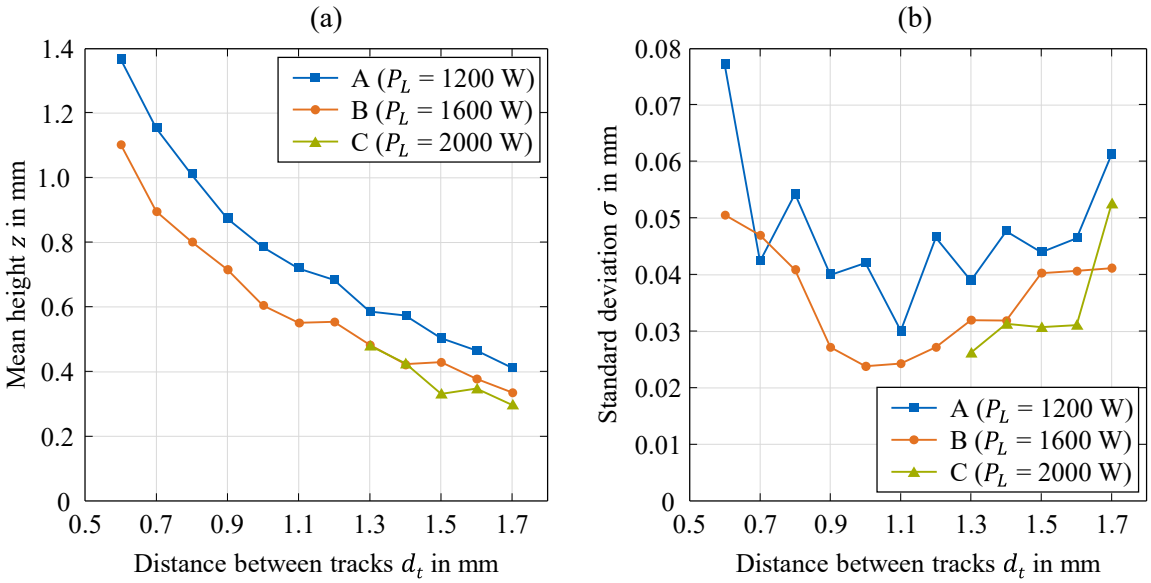

Figure 5: Mean heights (a) and standard deviations (b) of the z-coordinates for samples resulting from the test series with parameter sets A, B, and C

In Figure 6, the surface topographies of the samples obtained for the minimum (Figure 6a), the maximum (Figure 6b), and the optimum (Figure 6c) track distance when using parameter set B are displayed. For the minimum track distance, a gradual increase in the height is apparent in the initial region (left) due to the large overlap. At the maximum track distance, the valleys between the beads are clearly visible, while at the optimum track distance, the surface is comparably smooth and exhibits a uniform height. The resulting dilution will not be considered further in this work since the main focus is not on coating applications but on additively building up 3D structures.

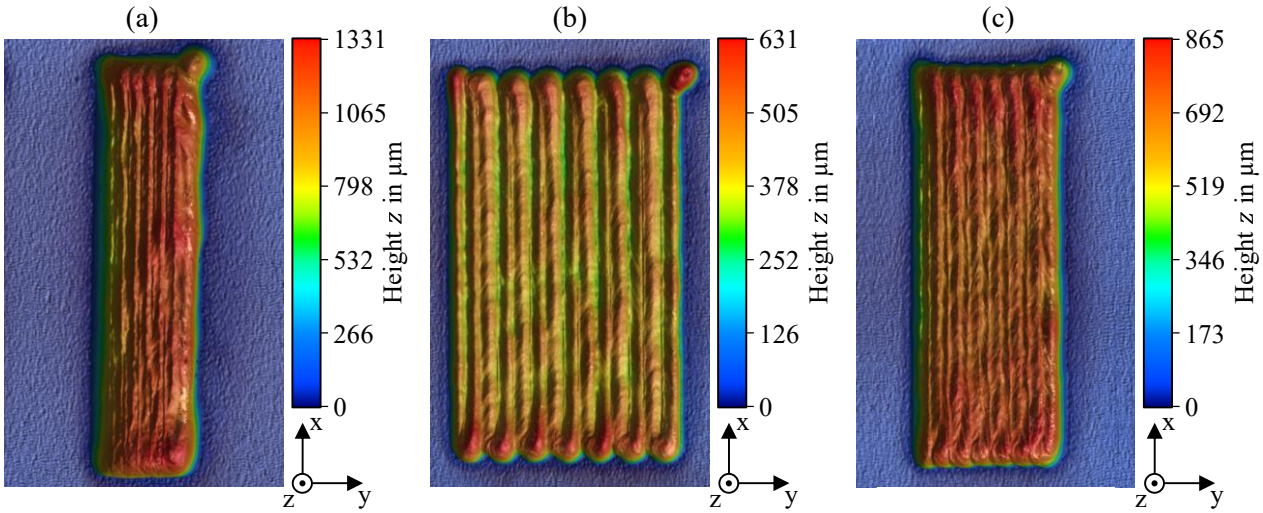

Figure 6: Surface topographies of samples produced using parameter set B: (a) 0.6 mm track distance, (b) 1.7 mm track distance, (c) 1.0 mm track distance

Deposition of Multi-track Multi-layer 3D Geometries. Using the determined optimal track distance of 1 mm for parameter set B, several cuboids were produced. The orientation of the layers was rotated by 90° in an alternating manner to avoid amplifying defects that might be present in the previous layers [8, 27]. Particularly with industrial robots, which are frequently deployed in LMD processes due to their high flexibility, the existing dynamic constraints must be considered. For example, sharp corners can only be traced precisely by stopping at the edge and accelerating again. Since the wire feed rate remains constant, there will be a material accumulation in this corner area. When building a cuboid using the chosen zigzag deposition pattern, this leads to a collapse in the center, as shown in Figure 7a. However, common robot controllers provide various interpolation methods to avoid such a full stop of the robot. When using a velocity criterion for the interpolation, falling edges developed after a few layers, see Figure 7b.

Finally, a strategy in which 20 % of the corners in the zigzag pattern were interpolated, proved to be effective. With this approach, as shown in Figure 7c, stable walls of the cuboid and an approximately flat surface could be achieved. The cuboid consisted of 32 layers with a base area of 50 mm×50 mm. In terms of the height increment after each layer, sound results were obtained for a value of 0.78 mm. This increment was slightly higher than the mean height of the first layer, which is related to the additionally deposited material resulting from the described path strategy at the corners.

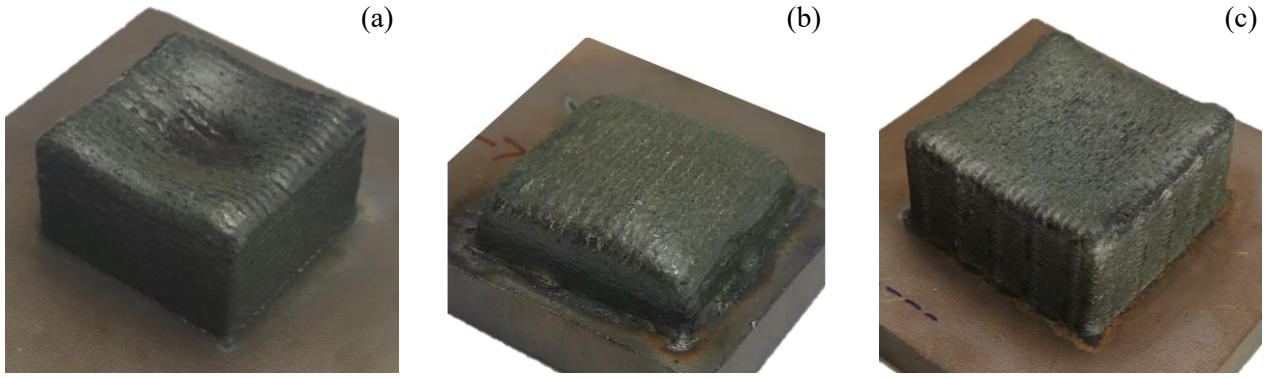

Figure 7: Built-up cuboids; (a) depression in the center, (b) falling edges, (c) defect-free build-up

Figure 8 shows a cross-section of the generated cuboid depicted in Figure 7c, with certain areas magnified in the detailed views. At the transition to the substrate, there is only a small heat-affected zone, which indicates only minor damage to the substrate material due to the process. In the detailed

view on the upper right, the individual layers are clearly visible. Throughout the whole cross-section, a sound bonding of the individual layers can be seen, with no distinct pores apparent. However, some inclusions are clearly visible, as exemplarily illustrated in the detailed view on the left. It is assumed that these inclusions are oxide layers formed during the process, which remained in the component when a new layer was applied. This hypothesis is supported by an EDS analysis performed. While no oxygen was detected in the additively built-up material at point B, an oxygen content of 34.9 wt% was measured inside the inclusion at point A. In order to avoid the formation of such oxide layers and thus their remaining inside the component, further improvement of the local shielding gas coverage through an optimized nozzle should be considered.

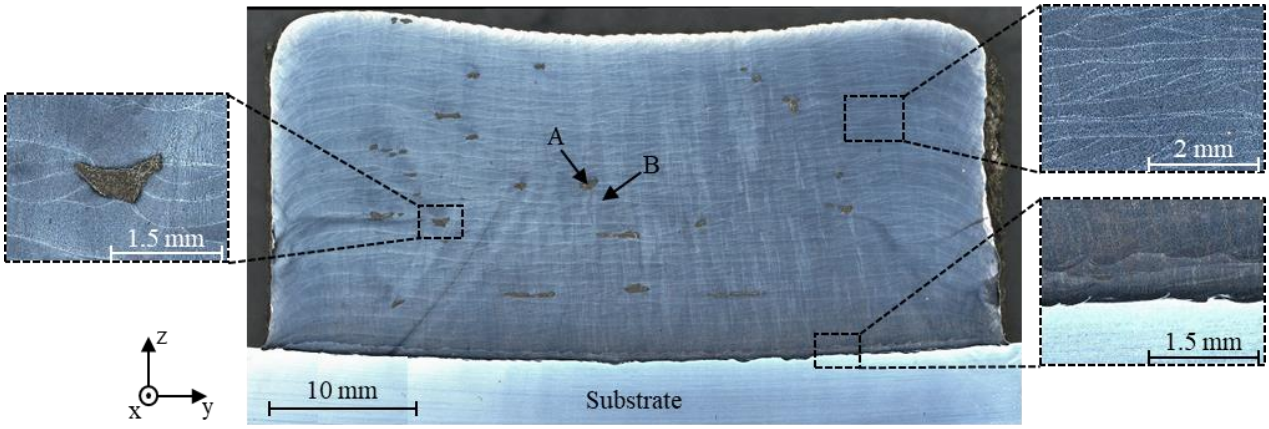

Figure 8: Cross-section of the multi-track multi-layer cuboid shown in Figure 7c together with various detailed views of relevant areas

Evaluation of the Melt Pool Temperature during the Deposition. The pyrometer integrated into the laser processing head was used to measure the melt pool temperature T_m during the build-up of the cuboid shown in Figure 7c. The obtained temperature curve is plotted in Figure 9. The sampling rate for the data acquisition was 47 Hz. To reduce noise, the signal was subsequently smoothed employing a lowpass filter with a passband frequency of 5 Hz.

In the temperature curve, an increasing trend can be observed during the first 480 s approximately, corresponding to the first six layers, until the average temperature remains almost constant. This initial increase results from the increasing heat accumulation in the part [28]. The melt pool temperature thus serves as an indicator of the thermal energy within the part. The detailed view in Figure 9 shows the temperature curve during the deposition of the second and the third layer. In the signal, periodic oscillations are apparent. These oscillations result from the zigzag deposition pattern, with two successive passes within a short time occurring after each change of direction in the outer areas. Due to the limited cooling rate of the deposited material, this leads to peaks in the temperature signal. Moreover, the transition between the layers is clearly visible, as the average temperature level changes abruptly at this point. In summary, the temperature curve clearly shows that process-related irregularities occur during the build-up of solid components. If more pronounced, these can lead to defects in the part. Therefore, they should be compensated for through an adaptive process control.

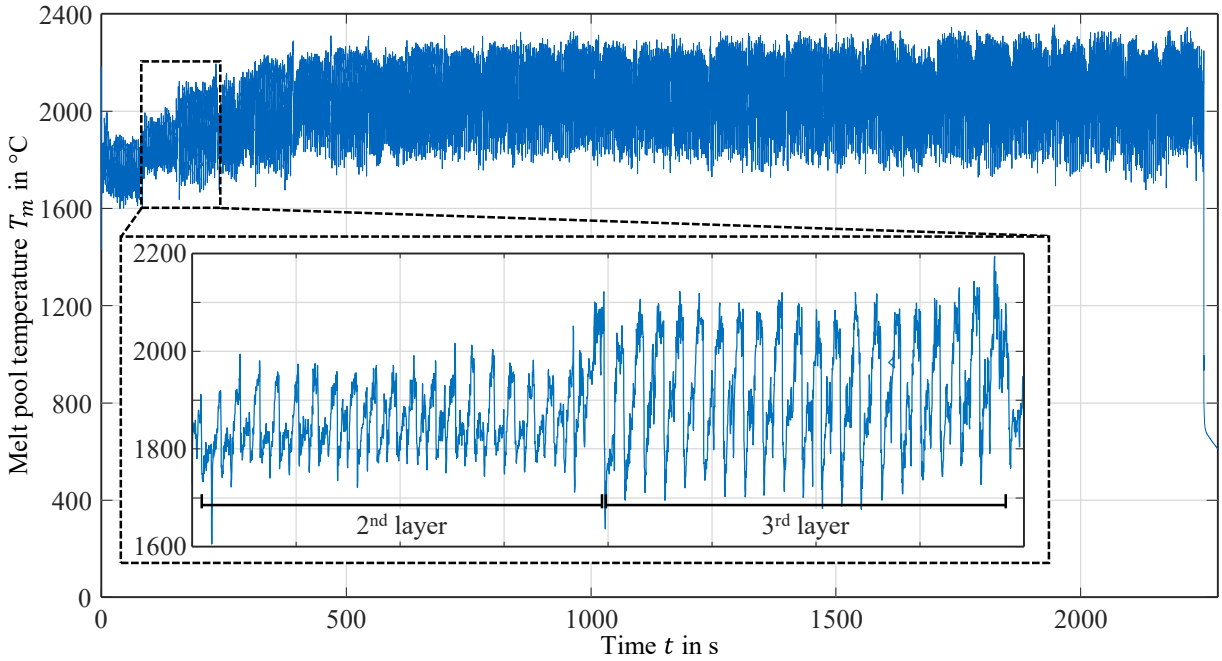

Figure 9: Melt pool temperature during the build-up of a cuboid together with the detailed signal representing two layers

A Novel Concept for Multivariable Process Control

The investigations on the build-up of a solid cuboid show that despite the advantages of coaxial wire feeding, there are several process-related challenges. In particular, geometries more complex than the presented cuboid require a great deal of effort to find adequate process parameters. If the parameters are not precisely tuned, defects due to overheating or deviations between the actual and the theoretical layer height can occur. To reduce the effort for parameter studies and thus to further establish wire-based LMD in industrial applications, an increased degree of automation is of crucial importance. For this reason, in-process monitoring and control are required for geometrically and structurally reliable components. It is therefore essential to obtain feedback from the process in real-time. Several process variables that can be measured online are feasible for this purpose. Of these, the melt pool temperature and the height of the applied layers are among the most relevant for process stability [29]. More significant deviations of these variables from the desired state inevitably lead to an unstable process and, consequently, to defective components. Both the melt pool temperature and the height of the part are virtually in all cases measured through optical methods, given that tactile measurements are impractical due to the high temperatures occurring in the process [30].

For monitoring the melt pool temperature in LMD processes, pyrometers as well as infrared (IR) cameras are suitable. Both sensors can be coupled into the beam path of the laser processing head. Thus, the freedom of movement is not restricted by additional external components, and direction-independent data acquisition is possible. This has been used to successfully control the melt pool temperature [31–33] as well as the closely related melt pool geometry [34–36] in different LMD processes, whereby the laser power was used as the manipulated variable.

For the height of the part and its topography, measurement systems based on laser triangulation or structured light projection are commonly used [14]. However, due to the directional dependency and the process emissions, online measurement is challenging, which is why measurements are usually performed after a layer has been applied. Thus, various layer-to-layer control systems have been developed employing such sensors [37–39]. Moreover, several authors have used laterally arranged CCD, CMOS, or IR cameras to detect the height of the bead or the part, respectively [40–42]. This method faces the challenge of accurately detecting the boundaries of the layer due to the intense illumination and fumes.

As was pointed out, an unstable process and thus defects can result from various causes that are independent of one another. To compensate for all significant disturbances, a simultaneous adjustment of different process parameters is desirable. Since there are considerable cross-couplings between the measured variables, several independent closed-loop controllers are not suitable in most cases. So far, there are only a few approaches for multivariable process control in LMD processes [40, 43]. Particularly, in wire-based LMD, real-time multivariable control has not yet been implemented. This is primarily due to the fact that real-time measurements of the layer height are a major challenge. In the following, a novel concept for the data acquisition and subsequently a multivariable process control is presented.

Direction-independent Monitoring in Real-time. A laser processing head with an annular beam profile is particularly suitable for monitoring wire-based LMD, since, in addition to a direction-independent process, this also enables direction-independent measurements. Therefore, the system used in this work will be equipped with further sensor technology in addition to the existing pyrometer.

To enable a highly accurate measurement of the layer height h_p in real-time, optical coherence tomography (OCT) represents a highly promising alternative to the existing approaches described above. This sensor technology based on low-coherence interferometry (LCI) is already established in several laser material processing applications [44, 45]. By splitting a coherent light beam, the relative distance between two reflecting surfaces can be determined based on the interference pattern of the reflected light beams [46]. The use of OCT for the height measurement in wire-based LMD offers several major advantages. On the one hand, interferometric measurements are not influenced by process-induced electromagnetic emissions [46]. On the other hand, by integrating the measurement principle into the laser processing head, a spatially lean solution is achieved that does not limit accessibility. Furthermore, a direction-independent measurement can be ensured with an annular beam profile by rotating the OCT spot using a scan system.

In combination with an in-axis pyrometer or an in-axis IR camera, which both allow a direction-independent measurement, an industrially applicable solution for the real-time acquisition of the part height and the melt pool temperature can thus be implemented.

Multivariable Closed-loop Process Control. The presented process monitoring system can ultimately be used for a closed-loop multivariable process control. The proposed control architecture to be implemented in future work is displayed in Figure 10. In the control architecture, the melt pool temperature and the part height are the controlled variables. The laser power P_L and the wire feed rate v_w are suited as the manipulated variables, as these significantly influence the melt pool temperature and the part height, respectively, and can be adjusted with a small time delay. With regard to the controller design, it is crucial to first determine a valid system model that maps the dynamic relationships between the input variables and the output variables, i.e., the manipulated variables and the controlled variables. In particular, it must be considered that significant cross-couplings are to be expected in the system. For example, a higher melt pool temperature can result in a broader and flatter melt pool, while the part height affects the focal position and thus the intensity of the laser radiation. These cross-couplings subsequently also have to be taken into account by the control algorithm. For this purpose, different approaches will be investigated, such as a decoupling structure in the controller, multivariable model predictive control (MPC), or machine learning approaches. With the described holistic control approach, a real-time multivariable control for wire-based LMD will be implemented for the first time, thus taking a significant step towards further establishing the process in industrial applications.

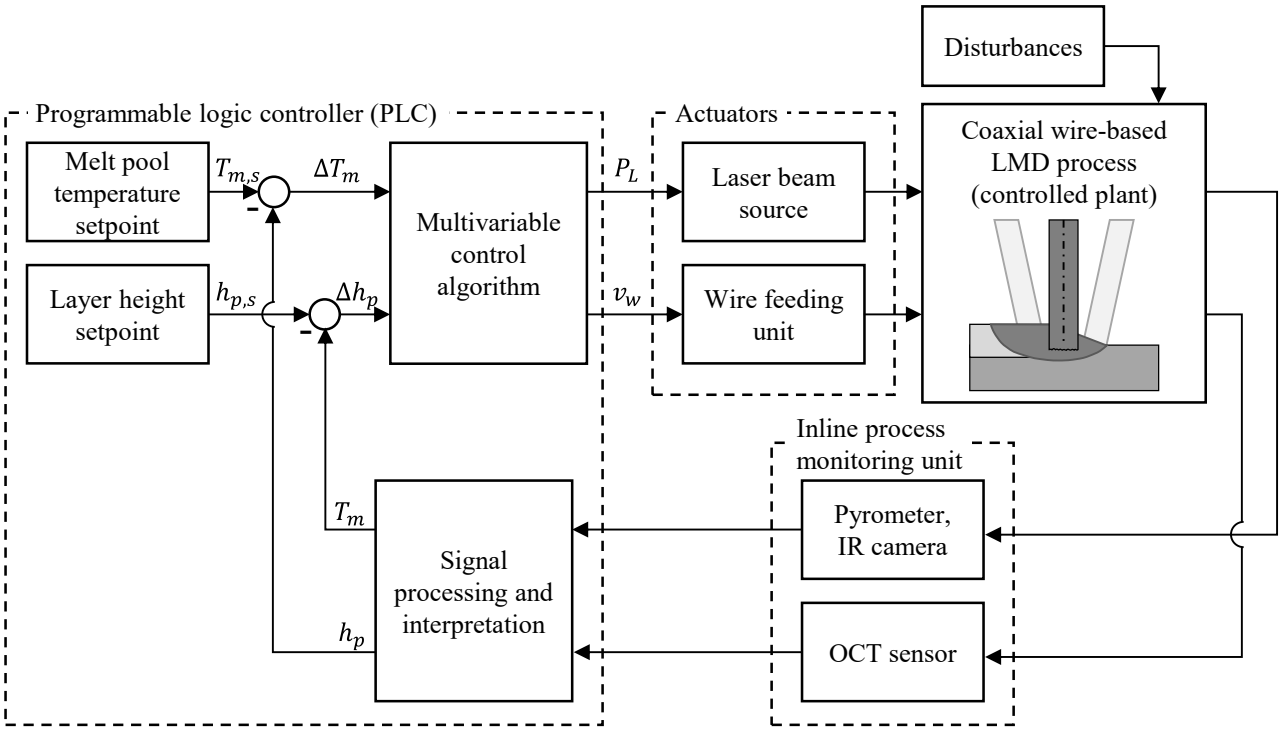

Figure 10: Architecture of the multivariable closed-loop process control with the LMD process as the controlled plant

Conclusions

In this study, process strategies for the defect-free build-up of solid metal parts by coaxial wire-based laser metal deposition were evaluated. As a key factor for the deposition of sound layers, the distance between adjacent weld beads was varied for different parameter sets. The produced samples were analyzed with respect to the resulting surface waviness. It was found that there is an optimum for the track distance, which deviates significantly from the theoretical optimum. This is because process-related physical phenomena are not considered in the common model. Furthermore, the amount of energy introduced into the part must be carefully monitored compared to single-track beads to avoid defects resulting from overheating. The optimum track distance determined, together with a precise tuning of the traverse speed at corners and the height increment, enabled the production of solid cuboids. Based on the results obtained, it can be concluded that both the part height and the melt pool temperature are crucial for a stable process and thus defect-free parts. Therefore, a novel concept for process monitoring using optical coherence tomography and IR temperature measurements as well as for a multivariable process control was developed. This concept will be implemented in future work. The control system is intended to be applied to solid and thin-walled structures. In this context, in-depth investigations of the mechanical and microstructural part properties will also be performed. The findings of this work represent a major step for the industrial advancement of coaxial wire-based laser metal deposition, which constitutes a promising alternative to the powder-based process variants.

Acknowledgments

Most of the results presented were achieved within the AdDEDValue project, which is supported by the German Federal Ministry for Economic Affairs and Climate Action (BMWK) within the funding program “Digitalization of Vehicle Manufacturers and the Supplier Industry” (contract number 13IK002L) and supervised by the VDI Technology Center (VDI TZ). We would like to thank the BMWK and the VDI TZ for their support and for the effective and trusting cooperation.

References

[1] A. Dass, A. Moridi, State of the Art in Directed Energy Deposition: From Additive Manufacturing to Materials Design, Coatings 9 (2019) 7, pp. 418.

[2] T. DebRoy, H.L. Wei, J.S. Zuback, T. Mukherjee, J.W. Elmer, J.O. Milewski, A.M. Beese, A. Wilson-Heid, A. De, W. Zhang, Additive manufacturing of metallic components – Process, structure and properties, Progress in Materials Science 92 (2018), pp. 112–224.

[3] E.W. Teichmann, J. Kelbassa, A. Gasser, S. Tarner, J.H. Schleifenbaum, Effect of wire feeder force control on laser metal deposition process using coaxial laser head, Journal of Laser Applications 33 (2021) 1, pp. 12041.

[4] B.T. Gibson, Y.K. Bandari, B.S. Richardson, A.C. Roschli, B.K. Post, M.C. Borisch, A. Thornton, W.C. Henry, M. Lamsey, L.J. Love, Melt pool monitoring for control and data analytics in large-scale metal additive manufacturing (2019).

[5] M. Bambach, I. Sizova, F. Silze, M. Schnick, Comparison of laser metal deposition of Inconel 718 from powder, hot and cold wire, Procedia CIRP 74 (2018), pp. 206–209.

[6] S. Ji, F. Liu, T. Shi, G. Fu, S. Shi, Effects of Defocus Distance on Three-Beam Laser Internal Coaxial Wire Cladding, Chin. J. Mech. Eng. 34 (2021) 1.

[7] M. Lammers, K. Biester, N. Schwarz, J. Hermsdorf, S. Kaierle, H. Ahlers, Automatic changing of weld deposit for additive manufacturing of hybrid metal-glass components using direct laser deposition, Lasers in Manufacturing Conference 2021 (2021).

[8] M. Madarieta-Churruca, J. Pujana-Astarloa, I. Garmendia Saez-de-Heredia, J. Leunda-Arrizabalaga, Additive Manufacturing of Metal Components Using Concentric-Wire Laser Metal Deposition, DYNAII 93 (2018) 1, pp. 675–680.

[9] J. Kelbassa, O. Pütsch, A. Gasser, A. Biber, K. Wissenbach, P. Loosten, J.H. Schleifenbaum, Influence of focal length on the laser metal deposition process with coaxial wire feeding (2019), pp. 11.

[10] M. Motta, A.G. Demir, B. Previtali, High-speed imaging and process characterization of coaxial laser metal wire deposition, Additive Manufacturing 22 (2018), pp. 497–507.

[11] E. Govekar, A. Kuznetsov, A. Jerič, Drop on demand generation from a metal wire by means of an annular laser beam, Journal of Materials Processing Technology 227 (2016), pp. 59–70.

[12] G. Zhu, D. Li, A. Zhang, G. Pi, Y. Tang, The influence of laser and powder defocusing characteristics on the surface quality in laser direct metal deposition, Optics & Laser Technology 44 (2012) 2, pp. 349–356.

[13] S. Donadello, M. Motta, A.G. Demir, B. Previtali, Monitoring of laser metal deposition height by means of coaxial laser triangulation, Optics and Lasers in Engineering 112 (2019), pp. 136–144.

[14] I. Garmendia, J. Pujana, A. Lamikiz, M. Madarieta, J. Leunda, Structured light-based height control for laser metal deposition, Journal of Manufacturing Processes 42 (2019), pp. 20–27.

[15] D. Ding, Z. Pan, D. Cuiuri, H. Li, Wire-feed additive manufacturing of metal components: technologies, developments and future interests, Int J Adv Manuf Technol 81 (2015) 1-4, pp. 465–481.

[16] J. Shi, P. Zhu, G. Fu, S. Shi, Geometry characteristics modeling and process optimization in coaxial laser inside wire cladding, Optics & Laser Technology 101 (2018), pp. 341–348.

[17] H. Pajukoski, J. Näkki, S. Thieme, J. Tuominen, S. Nowotny, P. Vuoristo, High performance corrosion resistant coatings by novel coaxial cold- and hot-wire laser cladding methods, Journal of Laser Applications 28 (2016) 1, pp. 12011.

[18] L. Budde, M. Lammers, J. Hermsdorf, S. Kaierle, L. Overmeyer, Process development for laser hot-wire deposition welding with high-carbon cladding Material AISI52100, Lasers in Manufacturing Conference 2021 (2021).

[19] J. Kelbassa, A. Gasser, J. Bremer, O. Pütsch, R. Poprawe, J. Henrich Schleifenbaum, Equipment and process windows for laser metal deposition with coaxial wire feeding, Journal of Laser Applications 31 (2019) 2, pp. 22320.

[20] S.H. Oliari, A.S.C.M. D'Oliveira, M. Schulz, Additive Manufacturing of H11 with Wire-Based Laser Metal Deposition, Soldagem & Inspeção 22 (2017) 4, pp. 466–479.
[21] Y. Li, Y. Sun, Q. Han, G. Zhang, I. Horváth, Enhanced beads overlapping model for wire and arc additive manufacturing of multi-layer multi-bead metallic parts, Journal of Materials Processing Technology 252 (2018), pp. 838–848.
[22] L. Nguyen, J. Buhl, M. Bambach, Multi-bead Overlapping Models for Tool Path Generation in Wire-Arc Additive Manufacturing Processes, Procedia Manufacturing 47 (2020), pp. 1123–1128.
[23] J. Xiong, G. Zhang, H. Gao, L. Wu, Modeling of bead section profile and overlapping beads with experimental validation for robotic GMAW-based rapid manufacturing, Robotics and Computer-Integrated Manufacturing 29 (2013) 2, pp. 417–423.
[24] D. Ding, Z. Pan, D. Cuiuri, H. Li, A multi-bead overlapping model for robotic wire and arc additive manufacturing (WAAM), Robotics and Computer-Integrated Manufacturing 31 (2015), pp. 101–110.
[25] S. Suryakumar, K.P. Karunakaran, A. Bernard, U. Chandrasekhar, N. Raghavender, D. Sharma, Weld bead modeling and process optimization in Hybrid Layered Manufacturing, Computer-Aided Design 43 (2011) 4, pp. 331–344.
[26] A. Zapata, C. Bernauer, M. Hell, M.F. Zaeh, Studies on the direction-independent temperature measurement of a coaxial laser metal deposition process with wire, Lasers in Manufacturing Conference 2021 (2021).
[27] N. Shamsaei, A. Yadollahi, L. Bian, S.M. Thompson, An overview of Direct Laser Deposition for additive manufacturing; Part II: Mechanical behavior, process parameter optimization and control, Additive Manufacturing 8 (2015), pp. 12–35.
[28] T. Hua, C. Jing, L. Xin, Z. Fengying, H. Weidong, Research on molten pool temperature in the process of laser rapid forming, Journal of Materials Processing Technology 198 (2008) 1-3, pp. 454–462.
[29] H. Wang, W. Liu, Z. Tang, Y. Wang, X. Mei, K.M. Saleheen, Z. Wang, H. Zhang, Review on adaptive control of laser-directed energy deposition, Opt. Eng. 59 (2020) 07, pp. 1.
[30] S.K. Everton, M. Hirsch, P. Stravroulakis, R.K. Leach, A.T. Clare, Review of in-situ process monitoring and in-situ metrology for metal additive manufacturing, Materials & Design 95 (2016), pp. 431–445.
[31] L. Song, J. Mazumder, Feedback Control of Melt Pool Temperature During Laser Cladding Process, IEEE Trans. Contr. Syst. Technol. 19 (2011) 6, pp. 1349–1356.
[32] G. Bi, A. Gasser, K. Wissenbach, A. Drenker, R. Poprawe, Characterization of the process control for the direct laser metallic powder deposition, Surface and Coatings Technology 201 (2006) 6, pp. 2676–2683.
[33] L. Tang, R.G. Landers, Melt Pool Temperature Control for Laser Metal Deposition Processes—Part I: Online Temperature Control, Journal of Manufacturing Science and Engineering 132 (2010) 1.
[34] B.T. Gibson, Y.K. Bandari, B.S. Richardson, W.C. Henry, E.J. Vetland, T.W. Sundermann, L.J. Love, Melt pool size control through multiple closed-loop modalities in laser-wire directed energy deposition of Ti-6Al-4V, Additive Manufacturing 32 (2020), pp. 100993.
[35] D. Tyralla, T. Seefeld, Temperature field based closed-loop control of laser hot wire cladding for low dilution, Procedia CIRP 94 (2020), pp. 451–455.
[36] M. Akbari, R. Kovacevic, Closed loop control of melt pool width in robotized laser powder–directed energy deposition process, Int J Adv Manuf Technol 104 (2019) 5-8, pp. 2887–2898.
[37] A. Heralić, Monitoring and control of robotized laser metal-wire deposition. Zugl.: Göteborg, Univ., Diss., 2012, Chalmers Univ. of Technology, Göteborg, 2012. ISBN: 978-91-7385-655-3.
[38] I. Garmendia, J. Pujana, A. Lamikiz, J. Flores, M. Madarieta, Development of an Intra-Layer Adaptive Toolpath Generation Control Procedure in the Laser Metal Wire Deposition Process, Materials (Basel, Switzerland) 12 (2019) 3.

[39] M. Buhr, J. Weber, J.-P. Wenzl, M. Möller, C. Emmelmann, Influences of process conditions on stability of sensor controlled robot-based laser metal deposition, Procedia CIRP 74 (2018), pp. 149–153.
[40] L. Song, V. Bagavath-Singh, B. Dutta, J. Mazumder, Control of melt pool temperature and deposition height during direct metal deposition process, Int J Adv Manuf Technol 58 (2012) 1-4, pp. 247–256.
[41] J. Flores, I. Garmendia, Cabanes Axpe, Thermal Monitoring and Control by Infrared Camera in the Manufacture of Parts with Laser Metal Deposition, DYNAII 95 (2020) 1, pp. 360–364.
[42] A. Fathi, A. Khajepour, E. Toyserkani, M. Durali, Clad height control in laser solid freeform fabrication using a feedforward PID controller, Int J Adv Manuf Technol 35 (2007) 3-4, pp. 280–292.
[43] Q. Wang, J. Li, M. Gouge, A.R. Nassar, P. Michaleris, E.W. Reutzel, Physics-Based Multivariable Modeling and Feedback Linearization Control of Melt-Pool Geometry and Temperature in Directed Energy Deposition, Journal of Manufacturing Science and Engineering 139 (2017) 2.
[44] C. Stadter, M. Schmoeller, M. Zeitler, V. Tueretkan, U. Munzert, M.F. Zaeh, Process control and quality assurance in remote laser beam welding by optical coherence tomography, Journal of Laser Applications 31 (2019) 2, pp. 22408.
[45] M. Schmoeller, C. Stadter, S. Liebl, M.F. Zaeh, Inline weld depth measurement for high brilliance laser beam sources using optical coherence tomography, Journal of Laser Applications 31 (2019) 2, pp. 22409.
[46] M. Kogel-Hollacher, M. Strebel, C. Staudenmaier, H.-I. Schneider, D. Regulin, OCT sensor for layer height control in DED using SINUMERIK® controller, in: H. Helvajian, B. Gu, H. Chen (Eds.), Laser 3D Manufacturing VII, SPIE, 2020 - 2020, 112710O-1 - 112710O-5. ISBN: 9781510633056.